Wideband Cyclostationary Signal Processing Using Sparse Subsets of Narrowband Subchannels

Chad M. Spooner, *Senior Member, IEEE,* Apurva N. Mody, *Senior Member, IEEE*

***Abstract*—The problem of signal detection and modulation recognition is addressed in both the blind and nonblind contexts. Many relevant modulation recognition algorithms have been created over the past three decades. The essential engineering trade-off that fuels the algorithm-invention process is between generality and optimality. Optimal (for example, maximum-likelihood) algorithms can be devised for narrow subsets of signal types, whereas highly general but suboptimal feature-based algorithms can be devised for wide subsets of types. It has previously been shown that cyclostationary-based classifiers possess highly desirable properties, such as tolerance to noise and cochannel interference, but also that they are computational costly and so are resistant to real-time hardware implementation. In this paper, we present a reduced-complexity method of signal detection and modulation recognition that exploits the cyclostationarity of over-the-air observed communication signals. The key idea is to represent wideband input data as a set of narrowband, contiguous, nonoverlapping subchannels, and then to extract the desired cyclostationary features for the wideband data using only sparse subsets of the subchannels.**

***Index Terms*—Blind Modulation Recognition, Cyclostationary Signal Processing, Filterbank Channelizer, Spectral Correlation, Cyclic Cumulants, Tunneling, Spectrum Sensing, Cognitive Radio**

I. Introduction

AUTOMATIC and general radio-frequency scene analysis (RFSA) is a type of signal analysis that is traditionally associated with spectrum monitoring and surveillance. Like other kinds of scene analysis—acoustic, dramatic, crime—the ideal form of RFSA provides a comprehensive assessment of the scene, resulting in a description that contains all relevant details as well as higher-level assessments. Recently RFSA has become important in the commercial communications world as an enabling technology for cognitive radio (CR) [3]–[10].

A general RFSA algorithm must contend with a wide variety of RF scenes, including the nominal case of a single weak primary-user (PU) signal, as well as cases involving cochannel interference (CCI), signals of unknown type, and signals impaired by transmitter imperfections and propagation-channel conditions. Restricted versions of the RFSA problem are amenable to mathematical optimization, such as when the universe of signals comprising the scene is restricted to digital quadrature amplitude modulation (QAM) with square constellations. More general versions are mathematically intractable and suboptimal feature-based algorithms are typically devised [11]. A class of useful feature-based algorithms exploits signal cyclostationarity (CS) because CS features are relatively insensitive to noise and CCI, and because almost all communication signals exhibit the property [32]–[47].

A persistent drawback preventing widespread adoption of blind CS-based RFSA systems is large computational cost and large required system memory. The purpose of this paper is to describe a new approach to CS-based RFSA in which the computational cost is lowered sufficiently to permit implementation on hardware platforms such as FPGAs. The key innovation is to apply a channelizing operation on the wideband (WB) input sample stream before any cyclostationary signal processing (CSP) algorithms are applied. The remainder of the processing extracts the CS features for any signals in the WB data but uses only operations on sparse subsets of the channelizer outputs.

The novel contributions of this paper are (1) introduction of a mathematical framework that relates the cyclostationarity of a spanning set of narrowband

C. Spooner is with NorthWest Research Associates, Monterey, California, 93940, USA e-mail: cmspooner@nwra.com. A. Mody is with BAE Systems, Merrimack, NH.

This research was developed with funding from the Defense Advanced Research Projects Agency (DARPA). The views, opinions, and/or findings contained in this article are those of the authors and should not be interpreted as representing the official views or policies of the Department of Defense or the U.S. Government.

(NB) subchannels to the cyclostationarity of the underlying WB signal, (2) a novel low-cost nonblind interference-tolerant detection algorithm for signals with known CS properties, (3) introduction of the cycle-frequency refinement technique of tolerating error in presumed known cycle frequencies, (4) a novel low-cost interference-tolerant detection algorithm for signals with unknown CS properties, and (5) a novel low-cost modulation-recognition algorithm for signals with unknown CS properties. This framework and these algorithms are developed to enable operation on a typical FPGA device (e.g., Virtex-6) where conventional CSP algorithms are prohibitively costly in terms of computational cost and required memory.

Material related to this paper was first published in [18]. Since then, the authors have also been awarded an international patent on this technology [1]. In [18] the basic approach of using spanning NB subchannels is presented, and the various component algorithms were described at a high level. In the present paper the algorithms are described in detail and their performance characterized by key assessments involving a wide variety of captured and simulated signal types. Moreover, we provide computational cost comparisons between the developed algorithm and a CSP-based reference algorithm suitable for FPGA implementation in the present paper; no quantitative cost comparisons were presented in [18].

The remainder of this paper is organized as follows. In Section II, we present the key RF scene difficulties that foil almost all optimal and feature-based recognition systems: CCI and overly simple signal models. Blind versus nonblind processing is discussed and the utility of CS features is illustrated with an example involving several captured signals, including ATSC-DTV, WCDMA, and CDMA-EVDO. The computational costs and memory requirements are reviewed for efficient blind and nonblind CSP estimators. Related work on energy-efficient CSP is discussed in Section III. The CS properties of over-the-air observed communications signals are discussed in Section IV. The central concept of the paper, WB-signal feature estimation using only selected NB subchannels, is introduced in Section V, where algorithms for nonblind and blind RFSA are also presented. A reference algorithm for performance comparison is sketched in Section VI. Section VII discusses the design parameters of the tunneling approach and the boundary conditions of this approach. Illustrative processing examples and Monte Carlo performance evaluations are presented in Section VIII. Expended-energy comparisons between the reference algorithm and the proposed algorithm are provided in Section IX, and concluding remarks are made in Section X.

For the reader's convenience we have listed in Table I the abbreviations used throughout this paper.

TABLE I
ABBREVIATIONS USED IN THIS PAPER.

AM	Amplitude Modulation
ATSC	Advanced Television Systems Committee
BPSK	Binary PSK
BT	Basic Tunneling
CC	Cyclic Cumulant
CCI	Cochannel Interference
CF	Cycle Frequency
CR	Cognitive Radio
CS	Cyclostationarity
CSP	Cyclostationary Signal Processing
CSSCA	Cross SSCA
DFI	Detected Frequency Interval
DSSS	Direct-Sequence Spread Spectrum
DT	Dual Tunneling
DTC	Dual-Conjugate Tunneling
ED	Energy Detection
FFT	Fast Fourier Transform
FM	Frequency Modulation
FPGA	Field Programmable Gate Array
FSM	Frequency-Smoothing Method
GMSK	Gaussian Minimum-Shift Keying
MCD	Incoherent Multicycle Detector
KT	Known Type
LTI	Linear Time-Invariant
MC	Monte Carlo
MAC	Medium Access Control
MCM	Multi-Carrier Modulation
MSSA	Multiple-Signal Scene Analyzer
NB	Narrowband
NC	Non-Conjugate
NOMAC	Modulated Signals with No MAC
OOS	Over-the-Air Observed Signals
PFFT	Polyphase FFT
PI	Prior Information
PSK	Phase-Shift Keying
PU	Primary User
QAM	Quadrature Amplitude Modulation
RA	Reference Algorithm
RFSA	Radio Frequency Scene Analysis
ROC	Receiver Operating Characteristic
SC	Spectral Coherence
SCF	Spectral Correlation Function
SSCA	Strip Spectral Correlation Analyzer
TSM	Time-Smoothing Method
UT	Unknown Type
WB	Wideband

II. Background and Motivation

In this section, we review the elements of the RFSA problem that present the most difficulty to the algorithm designer: CCI and inapplicable signal models. We then discuss blind and nonblind processing, illustrate the potential efficacy of CS features using observed signal data, and review the computational costs of standard CSP estimators.

This paper provides no tutorial or review of the basic parameters of CS. For definitions of and estimators for the spectral correlation function (SCF), spectral coherence (SC), cyclic temporal moment function, and cyclic temporal cumulant function (or *cyclic cumulant* (CC)), see [43], [48], and [49].

A. Cochannel Signals

We define cochannel signals as two or more signals whose temporal and spectral support intervals significantly overlap. In contrast, adjacent-channel signals are defined as signals with no spectral overlap, and arbitrary temporal overlap. Inclusion of temporal overlap is important because we wish the definition to encompass all those processing situations for which simple signal-separation approaches such as linear time-invariant (LTI) filtering and time gating are ineffective.

B. Modulated Signals with No Medium Access Control or Framing (NOMAC)

A key issue in the context of CR spectrum sensing and RFSA is the fidelity of the mathematical models for the signals of interest. Simpler models can lead to tractable optimization problems, whereas more complex (realistic) models prohibit the solution of optimization problems but can result in the identification of useful classification features. The majority of published work on modulation recognition uses a simple linear modulation model that encompasses some subset of digital QAM, digital phase-shift keying (PSK), frequency-shift keying, and staggered digital QAM signals. The model almost always includes independent and identically distributed symbols (which rules out pilot sequences), and no trace of an access mechanism—no framing, slotting, coding, hopping, etc. Such signal models are what one encounters in standard communication-theory textbooks, such as the excellent [56], and are referred to herein as *Modulated Signals with no Medium Access Control or Framing (NOMAC)*. However, such NOMAC signals are rarely found in practice.

The distinction between NOMAC signals and the signals in actual use is important because the two kinds of signals are typically quite different statistically. That is, the CS of over-the-air observed signals (OOS) is often much more complex (and exploitable) than that of the NOMAC signals. This topic is discussed more fully by the first author in [39], which provides several captured-data examples.

The RFSA algorithm presented in this paper does not ignore NOMAC signals. However, the main focus of our paper is on OOS (LTE, WCDMA, CDMA, ATSC, SATCOM etc.). Many of our simulation performance examples are based on such signals.

C. Blind Versus Nonblind Processing

In a CR context, the CR spectrum sensor is attempting to detect the presence of a PU signal about which much is known in advance. For example, in the 802.22 context [9], the sensor tries to detect the presence of ATSC-DTV [2] and wireless-microphone FM signals. Such signals adhere to publicly available standards. When any information about the signal to be detected is employed in the detection process, we refer to the resulting detection algorithm as nonblind. When no prior information (PI) is used, the algorithm is blind. To attain a high degree of energy efficiency and also high performance, we use as much PI as possible to diagnose the RF scene. After performing such nonblind processing, the more expensive and error-prone blind processing is applied. A substantial amount of processing energy can be saved by reserving the blind processing for only those frequency intervals of the WB input band for which no nonblind detection was declared.

D. The Utility of CSP

CSP can be highly effective for RFSA because different modulation formats produce different sets of cycle frequencies (CFs). In some cases, the *value of the CF* is itself valuable, as is the case for signals arising from standards like WCDMA, CDMA, LTE, and GSM. In other cases, it is the *pattern of CFs* that allows signal classification. For example, all

DSSS BPSK signals adhering to the conventional model produce the same basic pattern of noncon-jugate (NC) CFs: $\alpha = k/T_{data}$, with the strongest SCF magnitude typically occurring for $k = P$, where P is the processing gain $P = T_{data}/T_{chip}$, T_{data}^{-1} is the data rate, and T_{chip}^{-1} is the chip rate. Both of these aspects of CFs are exploited by the RFSA algorithm described herein. To illustrate the potential effectiveness of CSP using only captured signals, consider the RF scene in Figure 1.

The 50-MHz-wide scene contains isolated ATSC-DTV signals at ± 12 MHz and three cochannel signals near midband (0 Hz): CDMA-EVDO, WCDMA, and DSSS BPSK. The PSDs of the two DTV signals are nearly enough to classify their types, but the number and types of the signals near midband are not estimable from the power spectrum. However, all five signals produce distinct CFs, some NC and some conjugate, and an RFSA algorithm operating on these two two-dimensional functions could detect and group the CFs, leading to unambiguous detection and classification of all five signals. The essential problem of this paper is the large complexity of that process, which is costly both in terms of computing the functions from the input sample stream and in terms of the large memory size needed to accommodate the vector multiplications and FFT operations used in standard CSP estimators.

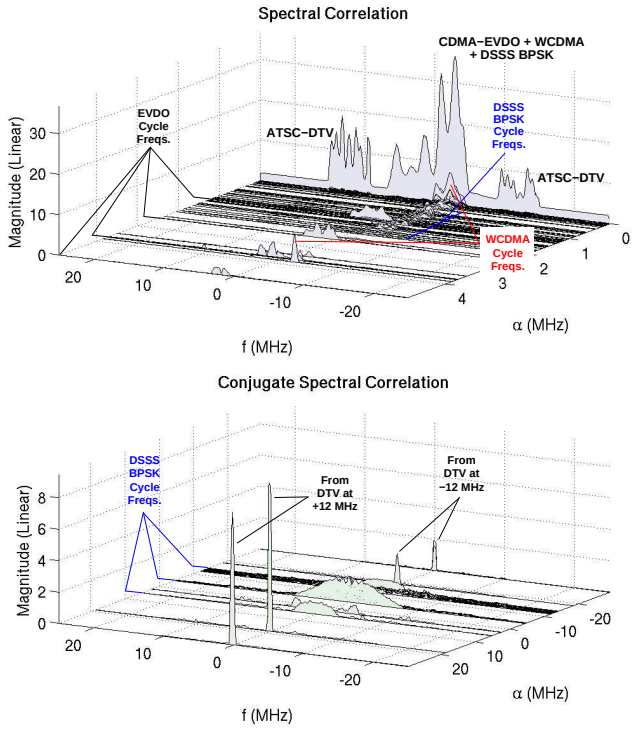

Fig. 1. Illustration of the spectral correlation feature separability for a complex RF scene involving five captured signals.

E. Computational and Storage Costs for Conventional CSP

The key SCF estimation algorithms are the frequency-smoothing method (FSM) [45], [49], time-smoothing method (TSM) [45], [49], and the strip spectral correlation analyzer (SSCA) [46], [47].

The FSM produces an estimate $\hat{S}_x^\alpha(t,f)$ of the SCF $S_x^\alpha(f)$ by smoothing the cyclic periodogram (CP) $I_{x,N}^\alpha(t,f)$,

$$\hat{S}_x^\alpha(t,f) = g_\Delta(f) \otimes I_{x,N}^\alpha(t,f), \quad (1)$$

where α is a CF, $g_\Delta(f)$ is a smoothing kernel with approximate width Δ, $\otimes$ denotes convolution, and the CP is defined by

$$I_{x,N}^\alpha(t,f) = \frac{1}{N} X_N(t, f+\alpha/2) X_N^*(t, f-\alpha/2), \quad (2)$$

and $X_N(t,f)$ is the Fourier transform of the data block $x(u)$ for $u \in [t-N/2, t+N/2]$.

For the FSM, the required length of the Fourier transform depends on the data-block length N. The TSM, on the other hand, uses a set of transforms of length N_T that is independent of the data block length,

$$\hat{S}_x^\alpha(t,f) = \frac{1}{M_1} \sum_{j=0}^{M_1-1} I_{x,N_T}^\alpha(t-N/2+jN_T, f) e^{-i2\pi\alpha j N_T}. \quad (3)$$

The TSM can be viewed as a generalization of the Bartlett spectrum estimator from stationary signal theory to CS theory. In the TSM, $N = M_1 N_T$. In the FSM, we define $M_2 = \lfloor N\Delta \rfloor$.

Another time-smoothing method is the SSCA, which produces the following cross SCF estimate between $x(t)$ and $y(t)$,

$$S_x^{f_k+q\Delta\alpha}(n, \frac{f_k}{2} - \frac{q\Delta\alpha}{2})_{\Delta t} = \sum_r X_{N_{chan}}(r, f_k) y^*(r) g(n-r) e^{-i2\pi qr/N}, \quad (4)$$

where N_{chan} is the size of a sliding Fourier transform that channelizes the data $x(t)$, N is the data-block length, $\Delta\alpha = 1/N$ is the CF resolution, and $\Delta t = N$. The SSCA first channelizes the scalar

input data with a relatively short FFT of length N_{chan}, then multiplies each channelizer output by the conjugated data $y(t)$ and a tapering window $g(t)$ (typically rectangular), and finally Fourier transforms the result. In terms of conventional notation, the frequency and CF parameters are related to the SCF point estimate by $f = (f_k - q\Delta\alpha)/2$, and $\alpha = f_k + q\Delta\alpha$, where $f_k = kf_s/N_{chan}$, $-N_{chan}/2 \leq k \leq N_{chan}/2 - 1$ are the center points of the channelizer output bands. Re-expressing this parameterization leads to $\alpha = 2f_k - 2f$, so that the point estimates for a single output Fourier transform lie along a line parallel to $\alpha = -2f$ in the (f, α) plane, which is called a *strip*. In the SSCA, we define $M_3 = N/N_{chan}$. For the auto-SSCA, $y(t) = x(t)$.

The three estimators are easily generalized to compute the *conjugate SCF* [48], [49].

The computational costs, in terms of complex multiplications, are graphed in Figure 2. We conclude that the FSM and TSM are vastly less complex than the SSCA in the case where the SCF is to be estimated for one or a few CFs, but that the SSCA is vastly less complex than the FSM and TSM when exhaustive coverage of the $f - \alpha$ plane is required. That is, the FSM and TSM are preferred for nonblind situations, in which one or more CFs are known in advance, and the SSCA is preferred in the blind situation, where no PI can guide the SCF estimation. The computational formulas for the basic versions of the three algorithms are given by [46], [47]

$$C_{FSM} = N\log_2(N) + 2N^2, \quad (5)$$

$$C_{TSM} = N\log_2(M) + 2N^2, \quad (6)$$

$$C_{SSCA} = NN_{chan}(\log_2(N_{nchan}) + 1). \quad (7)$$

and are plotted in Figure 2.

The memory costs for the FSM and SSCA are dominated by the large required N-point FFTs, whereas for the TSM the memory cost is much smaller since only small N_T-point FFTs are computed and accumulated. The variability of all the SCF estimates is inversely proportional to the time-frequency resolution product [43], which is $\Delta t\Delta f \approx M_i$ for the three cases, and also inversely proportional to SNR. This implies that for weak-signal or interference-limited cases, we must either increase the block size N, increase the frequency resolution, or increase both to obtain reliable SCF estimates. For the FSM and SSCA, this, in turn, implies that the FFT lengths must get longer, requiring ever more storage as SNR decreases. Fortunately, the TSM does not suffer from this increasing memory requirement and is therefore the most suitable for hardware implementation.

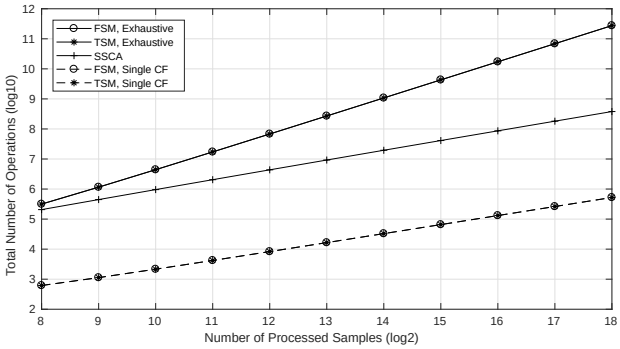

Fig. 2. Computational counts for key SCF estimators.

For a hardware implementation of an RFSA employing SCF estimators, it is preferable to use the TSM for all nonblind operations, and the SSCA using only relatively short data-block lengths for blind operations. We show in this paper that by combining front-end channelization, the TSM, and the cross SSCA (CSSCA), we can achieve this goal for a wide range of RFSA problems.

III. Related Work

There have been several attempts to significantly reduce the computational and memory costs associated with CSP. In [57], the emphasis is on low cost features and a hierarchical classification scheme. The first node in the classifier attempts to distinguish between all multicarrier modulations (MCM), such as all OFDM signals, and all single-carrier modulations, such as QAM, PSK, and DSSS signals. This decision is based on a single number, which is the fourth-order cumulant with two of the involved variables conjugated, or $C_{4,2}$ as it is commonly known. This statistic has several drawbacks, including that it is severely intolerant to CCI. The most serious problem, however, is that it appears to only work for simulated NOMAC signals. To test the $C_{4,2}$ statistic's ability to distinguish between $\{$OFDM$\}$ and $\{$DSSS, QAM, PSK$\}$, we applied the statistic to a set of OOS, including OFDM and DSSS, as well as to a set of simulated NOMAC signals, including OFDM, DSSS, and QAM/PSK. In all cases the inband SNR is greater than 20

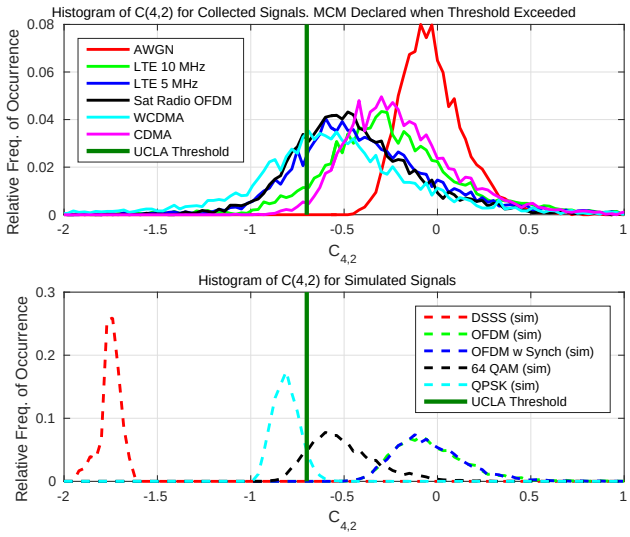

Fig. 3. Measured fourth-order cumulants for various captured and simulated communication signals using a block length of 128 samples. The UCLA energy-efficient spectrum sensing algorithm of [57] uses this cumulant to distinguish between multicarrier and single-carrier signals.

dB. The results are summarized in Figure 3. The statistic is unable to distinguish the two classes of signals drawn from captured data sets, but is able to distinguish OFDM from DSSS BPSK (but not from single-carrier signals) for NOMAC simulated data. In general, to perform blind RFSA, significantly more degrees of freedom are needed in the feature vector [36]–[38]. The CSP-based portions of the algorithm in [57] are likely effective when applied to suitable inputs, but we judged that a comparison of our overall RFSA algorithm to [57] is not of interest due to the performance of the MCM node.

In [19], the powerful concept of compressive sampling is applied to CSP. A key assumption in [19] is that the SCF is sparse in the CF dimension, although this is not quantified. To ensure sparsity in spite of this lack of quantifiability, the authors focus on WB NOMAC BPSK with rectangular pulse-shaping functions. Moreover, the cycle frequencies equal to the bit rate harmonics and doubled-carrier plus-and-minus the bit rate harmonics are ignored—the signal is treated as if it were statistically similar to amplitude modulation (AM) with a stationary modulating message. This is highly unrealistic for many OOS waveforms of interest, as is documented in detail in [23], [39].

A general CSP-based signal detector and classifier is derived in [37]. The algorithm is suitable for joint detection and classification of multiple cochannel signals and is therefore called the multiple-signal scene analyzer (MSSA). The MSSA is further analyzed and applied in [15], [23], [38], [39]. The key idea in the MSSA is CC matching, in which sets of nth-order CC magnitudes are blindly estimated from the data and compared to stored sets of CCs. The MSSA is compared to the tunnel-based algorithm of this paper in Section VIII.

IV. Cyclostationarity of OOS

Most OOS combine one or more underlying NOMAC signal types with an access mechanism, resulting in a transmitted signal that is markedly different from the NOMAC type. For example, GSM combines GMSK or $3\pi/8$-D8PSK with a TDMA access mechanism that includes eight user slots per GSM frame and a per-slot training sequence midamble. The NOMAC GMSK signal type possesses two cycle frequencies, but GSM possesses hundreds more [23], [39]. LTE, WCDMA, CDMA-EVDO, DVB-T and others behave similarly: they possess several-to-many CFs that are much smaller than the occupied signal bandwidth.

The case of captured 10-MHz LTE is illustrated in Figure 4. The signal possesses some strong features and many weak features, with CF values ranging from below 1 kHz to nearly the signal bandwidth of approximately 9 MHz. Many of the stronger features correspond to harmonics of 2 kHz. For these CFs, the corresponding SCF has a width nearly equal to the signal bandwidth. Therefore, the 4 kHz feature can be detected by considering virtually any pair of spectral components that are separated by 4 kHz. The entire signal bandwidth is not needed—only one or more NB spectral component pairs. The concept of exploiting a few such pairs, rather than processing the full-rate data, is called *tunneling*. Similar arguments hold for other WB signal types [39], [23].

V. Tunneling

The tunneling concept involves applying CSP to a few sets of NB subchannels (tunnels) to estimate the SCF or SC [18]. If the cost of channelization together with the tunnel-based CSP is smaller than the cost of full-rate processing, and the performance of the associated detectors and classifiers is comparable, then tunneling is more efficient than full-rate processing.

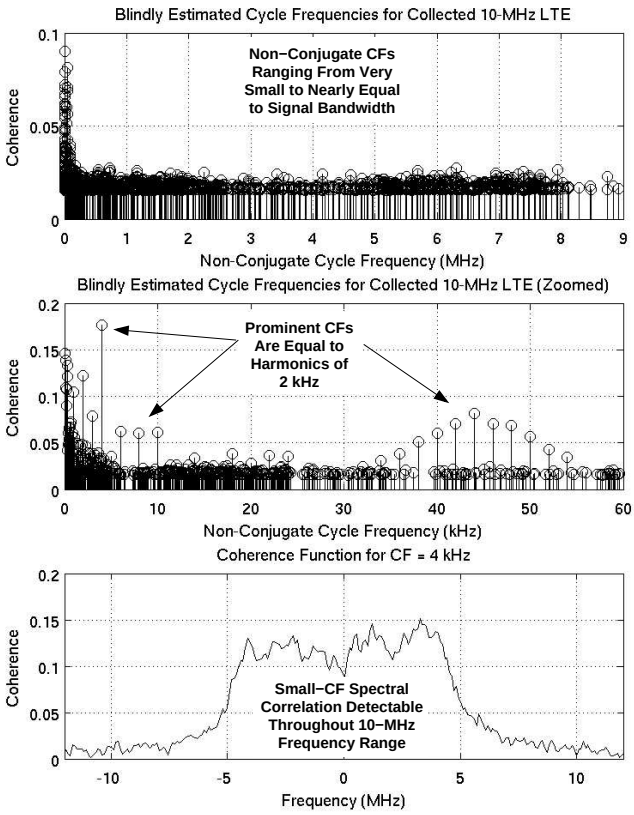

Fig. 4. Illustration of the CS of LTE (OFDM). The signal possesses a great many CFs that are orders of magnitude smaller than the signal bandwidth.

Let the complex-valued input data be denoted by $x(t)$, which is sampled at f_s Hz. The number of subchannels, or tunnels, is N_t and each has bandwidth $B_t = f_s/N_t$. The tunnels $y_k(t)$ are sampled at B_t Hz after downconversion to baseband, as indicated in Figure 5. Let the kth tunnel $y_k(t)$ correspond to center frequency f_k. Ideal tunneling consists of the equality

$$x(t) = \sum_{k=0}^{N_t-1} z_k(t) e^{i2\pi f_k t}, \qquad (8)$$

where $y_k(t) = z_k(tN_t)$. That is, the $z_k(\cdot)$ are high-rate low-pass subbands of the original data, and the $y_k(\cdot)$ are low-rate low-pass versions of the $z_k(\cdot)$. In practice, a filterbank is used to perform the channelization and the relation (8) holds approximately.

A. A Tunnel-Based Multistage Comprehensive Algorithm

The goal of the tunnel-based processing is to extract the same CS features as a full-rate CSP system would, but using only a small fraction of the N_t tunnels $y_k(t)$. An algorithmic approach to this goal is shown in Figure 6. The high-rate input signal is channelized to produce the parallel set of NB tunnels, and per-tunnel energy detection (ED) is applied to quickly find the strong signals. A simple noise-floor estimation algorithm is applied during production of the tunnel waveforms in the channelizer. The ED threshold is set 10 dB above the noise-floor estimate. No attempt is made to optimize this threshold; the idea is to reliably detect strong signals and produce very few false alarms. The large threshold also provides robustness to common non-flat noise-floor deviations such as tilts and ripples.

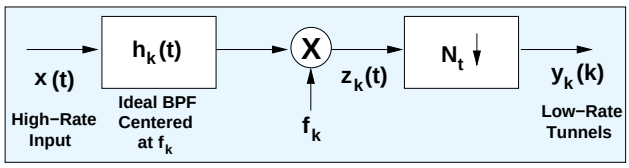

Fig. 5. Conceptual block diagram for creation of ideal tunnels.

The ED step is followed by nonblind processing which assesses the CS contained in the tunnels for each of a number of known CFs. Nonblind processing is followed by blind processing, which is broken into two steps. In the first step, the NC SC is applied to a subset of the tunnels to detect the presence of signal energy. The pattern of detected CFs across the analysis band $[-f_s/2, f_s/2)$ is then analyzed to yield a set of *detected frequency intervals* (DFIs). Finally, the tunnels comprising each DFI are jointly processed to classify and characterize the signal(s) residing in the DFI.

B. Creating Tunnels using Filterbank Channelizers

Our default channelizer is the polyphase FFT (PFFT) filterbank [21]. The PFFT produces the N_t tunnels at baseband, and is also used to spectrally whiten the data prior to further processing. Whitening is used in the front-end processing so that subsequent SCF estimates are approximately equivalent to coherence estimates. Coherence is preferred because it can be compared to a threshold that does not depend on the noise-floor or signal-power values [12].

C. Nonblind Tunnel-Based Signal Detection

The nonblind known-type (KT) signal detection step exploits prior knowledge of key CFs to detect

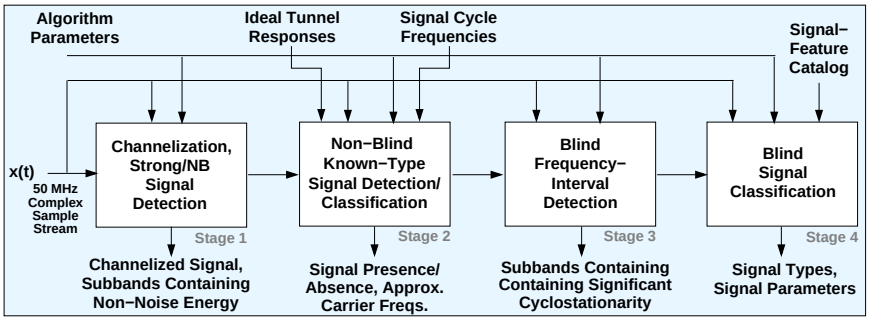

Fig. 6. Block diagram for a comprehensive signal-analysis system comprising both nonblind and blind elements.

the presence of standards-based signals such as WCDMA. The method of computing the detection statistic depends on the relationship between the known CFs $\{\alpha\}$ and the tunnel width B_t. For small NC CFs $\alpha < B_t$, the tunneling is referred to as *basic tunneling* (BT), for large NC CFs $\alpha > B_t$, the tunneling is *dual tunneling* (DT), and for all conjugate CFs, it is referred to as *dual-conjugate tunneling* (DTC).

1) Basic Tunneling: Basic tunneling exploits NC CFs, which must be smaller than B_t (Figure 7) For generic KT X, let the provided NC basic-tunneling CFs be denoted by $\{\alpha_{X,j}\}_{j=1}^{N_b}$. Then the basic-tunneling SCF measure for some arbitrary tunnel k is

$$Y_{b,X}(k) = \sum_{j=1}^{N_b} \left[\sum_f |\hat{S}_{x_k}^{\alpha_{X,j}}(f)| \right], \qquad (9)$$

where the SCF estimate is obtained using the TSM. The *basic-tunnel response* $\mathbf{Y}_{b,X}$ is the vector $[Y_{b,X}(1)\ Y_{b,X}(2) \ldots Y_{b,X}(N_t)]$. The *ideal basic-tunnel response* $\mathbf{I}_{b,X}$ is the basic-tunnel response obtained when the estimates $\hat{S}_{x_k}^{\alpha}(f)$ are replaced by their ideal values $S_{x_k}^{\alpha}(f)$. The BT statistic is an approximation to the maximum-likelihood-based incoherent multicycle detector [35].

The final step in BT is to convolve $\mathbf{Y}_{b,X}$ with $\mathbf{I}_{b,X}$, and to then find the maximum and its location in the result. The maximum constitutes a decision statistic and its location is used to determine the center frequency for signal X. To save energy, we compute only a subset of the $Y_{b,X}(k)$. Let the binary N_t-vector $\mathbf{S}$ have a one in the kth position if tunnel index k is used, else it is zero. Then for an arbitrary selection of employed tunnels in BT, the decision statistic is given by

$$Y_{basic,X} = \max\left[\mathbf{Y}_{b,X} * \mathbf{S}\right] \otimes \mathbf{I}_{b,X}, \qquad (10)$$

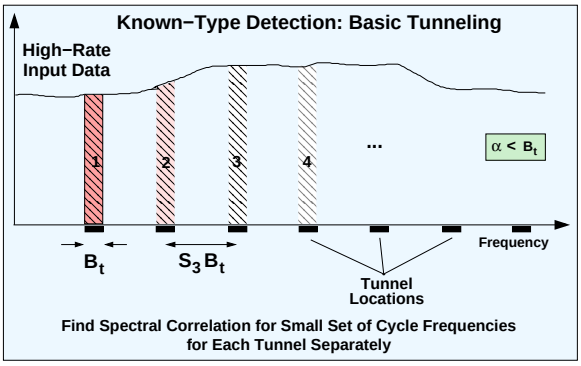

Fig. 7. Illustration of the KT detection method known as Basic Tunneling. S_3 is a *striding factor* that specifies the number of tunnels that are skipped between tunnel visits.

where $*$ denotes elementwise vector multiplication and $\otimes$ denotes convolution. Let the location of the maximum be $\hat{k}$, which is constrained to lie in the set $\{1, 2, \ldots, N_t\}$. Then the center-frequency estimate is $\hat{f}_c = f_s\left(\hat{k}/N_t - 0.5\right)$.

2) Dual Tunneling: It sometimes happens that the strongest features—that is, the slices of the SCF with the largest integrated magnitude over f—correspond to CFs that are much larger than the tunnel width B_t. These large CFs can also be exploited using tunneling, but a more complex algorithm is needed.

A large CF α can be exploited by correlating *pairs of tunnels separated by* α (Figure 8). The complicating factor is that the channelization produces regularly spaced NB components with separations $kf_s/N_t = kB_t$. If α is not equal to kB_t for some integer k, then the SCF for α cannot be accurately estimated by simple cross correlation involving two of the NB N_t data streams, because that would correspond only to a CF equal to kB_t.

The pairs of frequency components that we wish to correlate are contained in two separate tunnels,

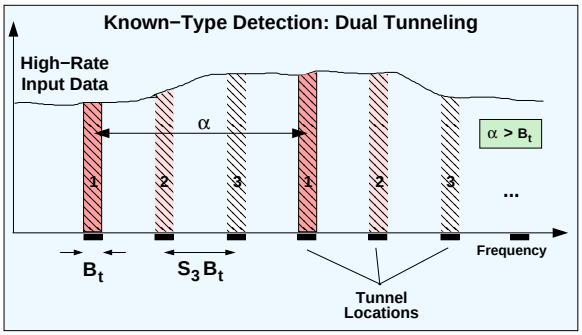

Fig. 8. Illustration of the KT detection method known as Dual Tunneling. S_3 is a *striding factor* that specifies the number of tunnels that are skipped between tunnel-pair visits.

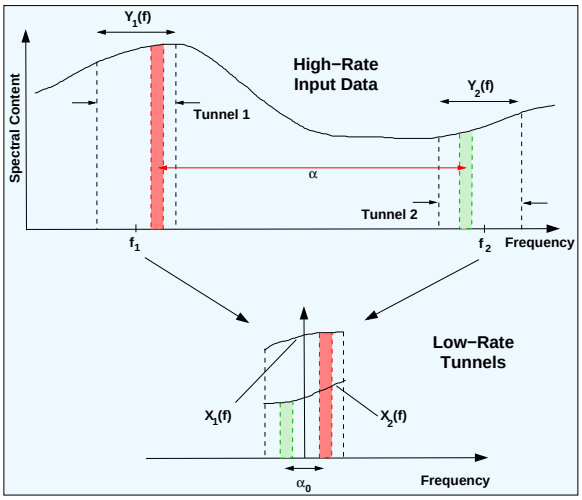

Fig. 9. Illustration of spectral components and tunnels found in dual tunneling.

and the index of the second tunnel is computable given the index of the first tunnel and the CF. Once the two tunnels are identified, then a cross SCF analysis can be performed to estimate the desired SCF. The remaining variable is the CF to use in the cross SCF analysis.

Suppose we have two tunnel indices k and l such that the set of frequencies corresponding to tunnel k is F_k and those for tunnel l are F_l. Further, suppose there is at least one frequency $f_k \in F_k$ and at least one frequency $g_l \in F_l$ such that $|f_k - g_l| = \alpha$. We seek the correlation between the frequency components with frequencies f_k and g_l, which can be computed by the spectral correlation between tunnels k and l ($l \geq k$) at CF $\alpha_0 = \alpha - (b_l - b_k)$, where b_l and b_k are the center frequencies for tunnels l and k, respectively (Figure 9).

Therefore, we may use tunnels to estimate the SCF for arbitrary CFs by picking the correct pairs of tunnels and estimating the cross SCF for the *residual* CF α_0.

For the kth tunnel index and KT X we define the spectral correlation measurement

$$Y_{d,X}(k) = \left[\sum_f |\hat{S}^{\alpha_{0,X}}_{x_k,x_l}(f)| \right]. \qquad (11)$$

where $x_k(t)$ is the kth tunnel, and $\hat{S}^{\alpha}_{x_k,x_l}(f)$ is the cross SCF estimate between the tunnels k and l obtained by a cross version of the TSM. If there is no index l less than N_t for a given index k and CF α, the dual-tunneling response for index k is defined to be zero.

The single-CF *dual-tunnel response* is the collection of these measurements,

$$\mathbf{Y}_{d,X} = [Y_{d,X}(1)\ Y_{d,X}(2)\ \ldots Y_{d,X}(N_t)]. \qquad (12)$$

To obtain the multiple-CF dual-tunnel response, each single-CF response is first circularly shifted by an amount equivalent to $\alpha/2$, and then these responses are added together. This shifting preserves the relationship between the response function and the physical frequencies involved in the tunnels.

The *ideal dual-tunnel response* $\mathbf{I}_{d,X}$ is the dual-tunnel response with $T \to \infty$. As in BT, we can elect to compute only some of the elements of $\mathbf{Y}_{d,X}$. The binary vector $\mathbf{S}$ selects which of the elements are computed. The final dual-tunneling statistic is then

$$Y_{dual,X} = \max[\mathbf{Y}_{d,X} * \mathbf{S}] \otimes \mathbf{I}_{d,X}. \qquad (13)$$

3) Dual-Conjugate Tunneling: In some important cases, a WB signal type cannot be successfully detected by either BT or DT because it does not possess significant NC CFs. Instead, it possesses only strong conjugate CFs. (An example is ATSC DTV [39].)

Conjugate CFs typically involve the carrier (center) frequency of the signal as well as a modulation rate, such as a chip rate or symbol rate. Therefore, prior knowledge of a conjugate CF amounts to prior knowledge of both the carrier frequency and one or more modulation rates.

The dual-conjugate tunneling concept is illustrated in Figure 10. Unlike the basic- and dual-tunneling algorithms, the DTC algorithm does not employ tunnel striding. Instead, it computes SCF estimates for a few tunnel pairs corresponding to spectral frequencies near zero.

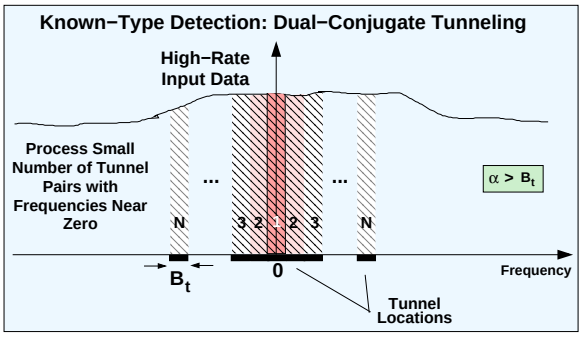

Fig. 10. Illustration of the known-type detection method known as Dual Conjugate Tunneling.

The DTC algorithm exploits the conjugate SCF, which correlates $X_{\Delta t}(t, f+\alpha/2)$ with $X_{\Delta t}(t, \alpha/2-f)^*$,

$$\hat{S}^{\alpha}_{xx^*}(f) = \langle X_{\Delta t}(t, f+\alpha/2) X_{\Delta t}(t, \alpha/2-f) \rangle \,. \tag{14}$$

For $f = 0$, this amounts to correlating $X_{\Delta t}(t, \alpha/2)$ with $X^*_{\Delta t}(t, \alpha/2)$, the conjugated version of itself. As f is increased, the involved NB spectral components move away from zero symmetrically, as shown in Figure 10. Because of this, all signals exhibiting conjugate spectral correlation have conjugate SCFs that are centered at $f = 0$.

Let the conjugate CF for KT X be denoted by α, and suppose the total number of tunnel pairs to consider is $2N_{dc}+1$ ($\ll N_t$). In practice, we are using shifted tunnels $X(t, f)$ and $X(t, \alpha - f)$, so we seek tunnel pairs symmetric around the tunnel corresponding to $f = -\alpha/2$ instead of $f = 0$. This center-point tunnel will have index k_0.

For any tunnel index k, we first find the index l for the tunnel that will be used to estimate the conjugate SCF. In dual tunneling, k and l were simply two tunnel indices whose center frequencies differed by approximately the cycle frequency of interest α. In DTC, the *sum* of the two tunnel centers is approximately equal to the CF. That is, suppose we have tunnel indices k and l such that there exists at least one frequency f_k in tunnel k and one frequency g_l in tunnel l such that $f_k + g_l = \alpha$. Then we can estimate the conjugate SCF by estimating the cross conjugate SCF for tunnels k and l using residual CF α_0 given by $\alpha_0 = \alpha - (b_l + b_k)$, where b_l and b_l are the center frequencies for tunnels l and k.

For dual-conjugate tunnel-pair indices k and l, and KT X, we compute the following integrated SCF statistic

$$Y_{dc,X}(k) = \sum_{j=1}^{N_{dc}} \left[\sum_{f} |\hat{S}^{\alpha_{0,X}}_{x_k, x_l^*}(f)| \right], \tag{15}$$

where the SCF estimate is obtained using a cross version of the TSM. The correlations are computed for all k in the set $\{k_0 + j\}_{j=-N_{dc}}^{N_{dc}}$, resulting in the vector of measured spectral correlation values given by

$$\mathbf{Y}_{dc,X} = [Y_{dc,X}(k_0 - N_{dc}) \;\; Y_{dc,X}(k_0 - N_{dc} + 1) \; \ldots \; Y_{dc,X}(k_0) \; \ldots \; Y_{dc,X}(k_0 + N_{dc})]. \tag{16}$$

This vector is the *dual-conjugate tunnel response*, and the *ideal dual-conjugate tunnel response* is the response for $T \to \infty$. The decision statistic is simply the maximum value of the convolution between the dual-conjugate response and its ideal version.

4) Cycle-Frequency Refinement: The KT signal detection approach adopted here will be effective if the sets of CFs assigned to each KT signal are actually exhibited by the transmitted signals. However, in practice, the assigned CFs can be different from the CFs exhibited by actual signals due to clock-frequency errors at the transmitter and/or at the receiver. Moreover, conjugate CFs are shifted by the Doppler effect. Other authors consider this potential CF mismatch to be fatal to CSP-based detection methods [14], [13], however, it is remedied by searching for a strong feature over CFs very near the assigned CF. This searching process results in a slight on-the-fly refinement of the CFs used for detection, and so is referred to as *CF refinement*. All known-type detection results and algorithmic cost estimates in this paper take into account CF refinement. Ten CFs near the putative known CF are included in every known-type TSM estimation.

5) Signal Presence Detection: Most signal types will yield a substantial tunnel response for only one of basic or dual tunneling, and dual-conjugate tunneling is used only when there is no other choice, as in the case of ATSC-DTV. In this research, we viewed each of the three distinct tunnel-based KT detectors as separate, and declare a signal is present if any one of them produces an output that exceeds an empirically determined threshold.

D. Blind Tunnel-Based Signal Detection

Once the KT signals are detected, and their center frequencies estimated, the spectral intervals over

which they reside can be estimated. To complete RFSA, the remaining portions of the input band can be examined for the presence of signals of unknown type (UT). Here *unknown type* is relative to the catalog of signal types known to the KT processor. The key concept is that the unknown signal types will exhibit at least one CF that is smaller than the tunnel bandwidth B_t. An exhaustive blind SCF estimator, the SSCA, is applied to a sparse set of tunnels that cover (span) the input-data bandwidth to obtain a list of detected NC CFs for each visited tunnel. This set of lists is then processed to estimate the frequency intervals (DFIs) over which signal energy is present.

E. Blind Tunnel-Based Signal Classification

If the blind detection step produces at least one DFI, the blind signal classification subalgorithm is invoked. This algorithm aims to blindly classify and characterize the signals residing in the DFIs. To perform this task, the full set of CFs for each DFI must be estimated using only the NB tunnels. Such processing requires application of the SSCA to a minimal set of tunnel pairs.

1) Blind Exhaustive Cycle-Frequency Estimation: The entire SCF for any particular DFI can be obtained by processing only the set of spanning tunnels (see Appendix A). This is done by estimating the SCF for each tunnel as well as all cross SCFs for each pair of tunnels. Typically each CF will appear in multiple cross and auto SCF estimates, so that obtaining the full set of CFs for the DFI requires processing some minimal set of tunnel pairs. The blind exhaustive CF estimator processes a specified set of tunnels and tunnel pairs, and provides as output a list of four-tuples $L_{nc} = \{f_j, a_j, c_j, s_j\}_{j=1}^{J_{nc}}$ for the NC SCF and a list $L_c = \{F_j, A_j, C_j, S_j\}_{j=1}^{J_c}$ for the conjugate SCF. All subsequent parameter estimation and signal classification is performed by processing these lists.

2) Level-0 Processing: Known Cycle Frequencies: In Level-0 processing, the obtained lists are examined for the presence of known CFs. This is similar to the KT detection in that PI for signals of interest is used. However, the CF comparison is computationally inexpensive, so that the number of KT CFs that can be examined is much larger here. The Level-0 processing serves two purposes: (1) detecting KT signals that were missed in the KT stage, and (2) expanding the number of KT signal types.

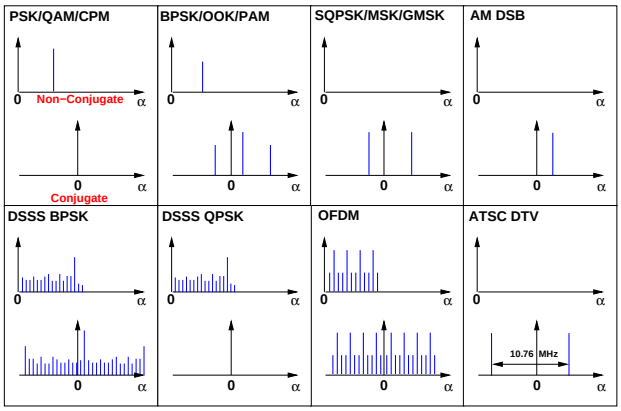

Fig. 11. Schematic illustration of various CF patterns.

3) Level-1 Processing: Cycle Frequency Pattern Detection: In the next stage of processing, the lists L_{nc} and L_c are processed to find one or more *CF groups*. Modulated signals exhibit sets of CFs that have recognizable patterns, such as those shown in Figure 11. A grouping algorithm was designed to automatically and blindly extract patterns such as these. If a pattern is detected, it can be processed to determine key signal parameters of interest, such as symbol rate, chip rate, and carrier frequency.

4) Level-2 Processing: Second- and Higher-Order Feature Classification: Second-order statistics are insufficient to unambiguously classify NO-MAC digital QAM, PSK, and CPM signals, since they have identical SCFs. When such a CF pattern is detected (upper left corner in Figure 11), the algorithm suite employs higher-order CCs to classify the modulation type. We have developed a method for estimating higher-order cyclic moments and cumulants using only operations on the DFI-spanning tunnels called the *cyclic moment phase* However, the classification method is highly sensitive to distortions in the front-end channelizer as well as signal distortions introduced by spectral whitening, and its performance is not included in this paper.

VI. A Reference Algorithm

A reference KT detection algorithm must perform KT signal detection using the same information as that supplied to the KT algorithm in Section V-C. That information consists of a small set of CFs and the corresponding SCFs. Unlike the developed

tunneling algorithm, the reference algorithm (RA) cannot take advantage of channelization (tunneling). An excellent choice for the RA is the incoherent multicycle detector (MCD) [35], which makes near-optimum use of the provided CF and SCF information. The MCD statistic is given by

$$Y_{MCD} = \sum_{\alpha \in A} \left| \sum_{f} \hat{S}_x^{\alpha}(f) S_s^{\alpha}(f)^* \right|, \qquad (17)$$

where $S_s^{\alpha}(f)$ is the ideal (theoretical) SCF, $\hat{S}_x^{\alpha}(f)$ is a measured SCF, α is a CF, and A is a small set of CFs specific to the signal of interest $s(t)$.

The MCD statistic works well when the center frequency of the signal is known. This permits the estimated and ideal SCFs in (17) to align in frequency. However, tunnel-based KT processing does not know the center frequency of the signal in advance and must estimate this parameter along with detecting the presence of the signal. Therefore, we use the *hopped* incoherent multicycle detector

$$Y_{HMCD} = \max_{f_0 \in F} \left[\sum_{\alpha \in A} \left| \sum_{f} \hat{S}_x^{\alpha}(f) S_s^{\alpha}(f - f_0)^* \right| \right], \qquad (18)$$

and the value of f_0 that achieves the maximum is used as a carrier-frequency estimate.

Due to the assumed hardware constraints, the reference-algorithm SCF cannot be estimated using the FSM, because it would require long FFTs whenever the desired processing length is long, as it is whenever the inband SNR is low. Instead, it is estimated using the TSM which can accommodate arbitrarily long sensing times using only short FFTs and an accumulator.

DFI detection is blind; it is not provided any PI on the signal environment. The RA must also be blind and is subject to the same hardware constraints as are adopted in the tunneling algorithm suite. The RA exhaustively searches the incoming high-rate data for the presence of NC CS. Due to the hardware constraints, it cannot do this using the SSCA, because low-SNR conditions would then require large strip FFTs in that algorithm. The TSM can accommodate any desired data length using only short FFTs and an accumulation operation. Since the tunnel-based DFI algorithm looks for NC CFs that are less than the tunnel bandwidth $B_t = f_s/N_t$ in magnitude, the RA will also search only for cycle frequencies in the range $(0, B_t]$. Therefore the reference algorithm will use the TSM and restrict the search to CFs less than B_t.

Finally, the MSSA of [37] is used in its nonblind mode as a further RA.

VII. Boundary Conditions for the Tunneling Approach

As discussed in the previous section, tunneling is a useful approach for low-energy spectrum sensing. The reduction in energy consumption is obtained by processing sparse subsets of narrow-band channels (e. g. 200 kHz tunnel instead of 10 MHz for LTE). This is carried out by detecting the CFs corresponding to slow moving features (for example the 0.5 ms sub-frame rate corresponding to a 2 kHz CF). This means that one can potentially detect the signal at substantially lower cost by processing a sparse subset of the band to be analyzed. For an LTE signal, assuming that each tunnel is approximately 200 kHz wide, this results in a 50-fold reduction in consumed energy.

In practice however, it is difficult to always obtain such large reduction in energy consumption while maintaining fairly large probability of signal detection. The probability of signal detection may suffer when the tunnel-striding parameter S_3 (see Figures 7 and 8) is large and the signal bandwidth is small. For example, the GSM signals are roughly 200 kHz wide. If the tunnel-striding parameter is 4 (only every fourth tunnel is considered) and the tunnel-width is 200 kHz, then there is a large probability that the signal will be missed. Similarly, the tunneling approach performs poorly against frequency hopping signals since the tunnel locations and widths are in general fixed.

Hence, the choice of parameters for the tunneling approach is determined by the types of signals that are likely to be found in the observations, probability of detection P_d vs probability of miss P_m vs probability of false alarm P_{FA} and, finally, the available computational resources.

Table II provides some insight into the design parameters and boundary conditions for the tunneling approach.

VIII. Performance

In this section, we provide illustrative and Monte Carlo (MC) performance examples that use OOS whenever possible.

TABLE II
DESIGN PARAMETERS THAT DETERMINE THE BOUNDARY CONDITIONS FOR THE TUNNELING APPROACH.

Parameter	Description	Performance Impacts
B_t	Tunnel Bandwidth	Larger: Poor CCI performance Smaller: Increases P_{miss}
S_3	Striding Factor	Larger: Increases P_{miss} Smaller: Needs more energy
Δt	Sensing Time	Larger: Increases P_d Smaller: Decreases P_d
Δf	Tunnel FFT Bin Size	Larger: Poor resolution Smaller: Needs more energy
$\Delta t \Delta f$	Time-Frequency Resolution	Must be $\gg 1$ for good P_d, P_{fa} tradeoff

Label	Type	Dominant CFs (MHz)
CDMA	CDMA 2000	1.25, 1.2288, 2.5
LTE 10 MHz	LTE	0.032,0.040,0.042
GSM	TDMA	0.01733,0.20,0.2708
WCDMA	UMTS	0.015, 0.12, 3.84
DSSS 10 MHz	BPSK (Sim)	0.0391, 10.0
DSSS 12.5 MHz	QPSK (Sim)	0.0245, 12.5
DSSS 20 MHz	BPSK (Sim)	0.0196,20.0
WiMAX FUSC	DL (Sim)	0.536
WiMAX OFUSC	DL (Sim)	0.0992
WiMAX PUSC	DL (Sim)	0.784
FH/DSSS Fast	Hopper (Sim)	0.0281
FH/DSSS Slow	Hopper (Sim)	0.619
Sat. Radio	Sirius/XM	2.53
LTE 5 MHz	LTE	0.004, 0.008, 0.10
CDMA EVDO	CDMA	1.23, 2.46, 3.69
Bluetooth	FH/PSK	1.0
DVB-T	Broadcast TV	0.054
TV Band 1	Unknown	0.383,0.778,1.556
TV Band 2	Unknown	0.0191,1.662

TABLE III
KNOWN-TYPE SIGNALS USED IN STAGE 3 PROCESSING.

Parameter	Value
Sample Rate	50 MHz
File Length (T)	5.4 sec
Block Lengths (T_b)	21, 42, 84, 168 ms
Tunnel BW (B_t)	200 kHz ($N_t = 256$)
Number of Trials	$\lfloor T/T_b \rfloor$
WCDMA SNRs	5, 10, 15, 20 dB
WCDMA CFs	15, 30, 120 kHz; 3.84 MHz
WCDMA Basic/Dual Stride	16/2
EVDO SNRs	2, 7, 12, 17 dB
EVDO CFs	1.23, 2.46, 3.69 MHz
EVDO Basic/Dual Stride	32/16

TABLE IV
MONTE-CARLO EXPERIMENT PARAMETERS FOR KNOWN-TYPE DETECTION OF COLLECTED WCDMA AND CDMA-EVDO SIGNALS.

A. Known-Type Detection: Comparison with References

The first example compares the detection and false-alarm performance for KT detection using the tunnel-based, reference, and MSSA algorithms. Over the air observed CDMA-EVDO and WCDMA signals are used[1]. For the tunnel-based and reference algorithms, the suite of known signal types are defined in Table III. Each known type is defined by one or more CFs.

In each MC trial, a random segment is extracted from a long OOS data file. The data samples are captured using a Tektronix RF Hawk signal analyer, which provides analog data at an intermediate frequency (IF) of 140 MHz, followed by a MaCOM downconverter, which shifts the data to an IF of 25 MHz, followed by a GE IP 1572 ADC sampler. Several segment lengths and SNRs are used in the MC experiment to allow presentation of probabilities that subsume several meaningful operational scenarios (see Table IV).

Receiver operating characteristics (ROCs) for the KT experiment are shown in Figures 12 and 13. Figure 12 shows the probabilities for the full experiment together with the RA (MCD) and the MSSA. The missed detections and the false alarms arise predominantly from the shortest block length (21 ms), as illustrated in Figure 13, which shows the probabilities for only the three largest block lengths. Evidently, the performances of the tunnel-based, reference, and MSSA algorithms are similar.

B. Known-Type Detection: Low SINR Cochannel Example

To illustrate the ability of the tunnel-based CSP-exploiting algorithm to detect multiple co-channel signals at low SINR, consider the case of five OOS signals that are shifted to a common center frequency and then added together. The resultant PSD is shown in Figure 14. The KT detection algorithm is applied to this scenario using a block length of 168 ms. The signals have equal average power levels, so that each experiences an SINR of about -6 dB. The red text in the figure shows the detected signals using the tunnel-based KT algorithm. The basic/dual stride factors are as follows: LTE 4/4, WCDMA 16/2, EVDO 8/8, CDMA 8/1. A total of nine tunnels are visited in the DTC algorithm for ATSC DTV. The tunnel responses are shown in

[1]The data can be obtained at the link in [58].

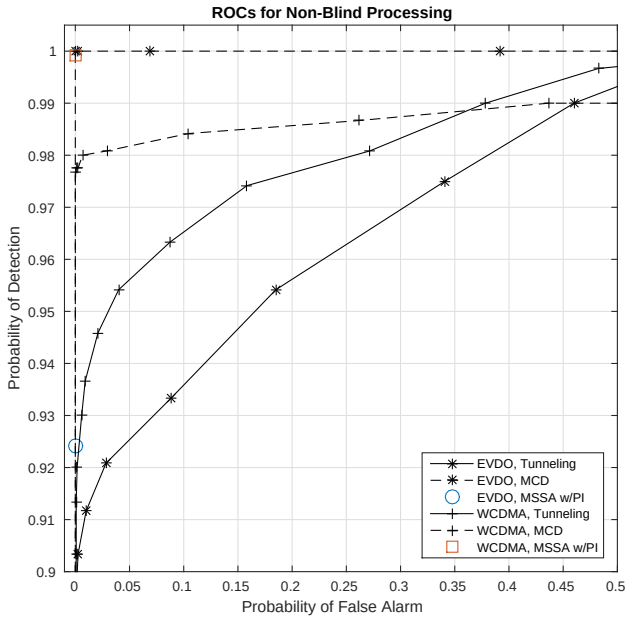

Fig. 12. ROCs for known-type processing. These ROCS correspond to averages over four different block lengths and several SNR values.

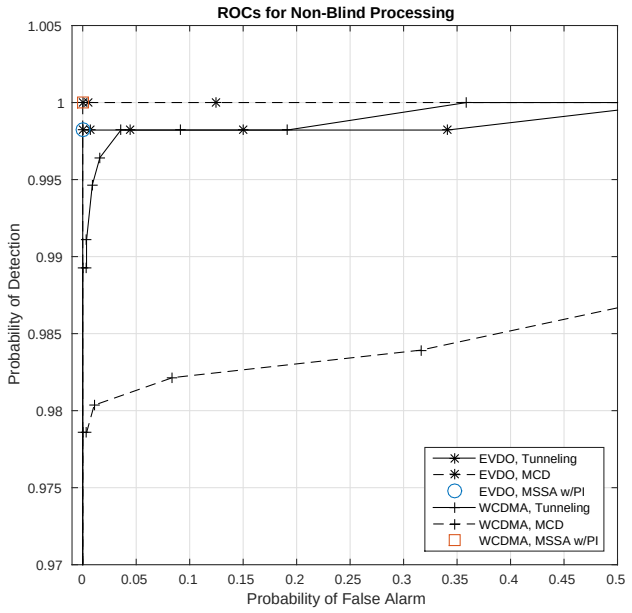

Fig. 13. ROCs for known-type processing. These ROCS omit the results for the shortest block length.

Figure 15. The data file for this example can be obtained from the link in [58].

C. Unknown-Type Detection and Classification

In this section, we present a performance example for blind signal detection and classification using Level-1 processing. The experiment uses synthetic NOMAC DSSS BPSK, DSSS QPSK, BPSK, QPSK, and MSK signals. Table V provides the parameters

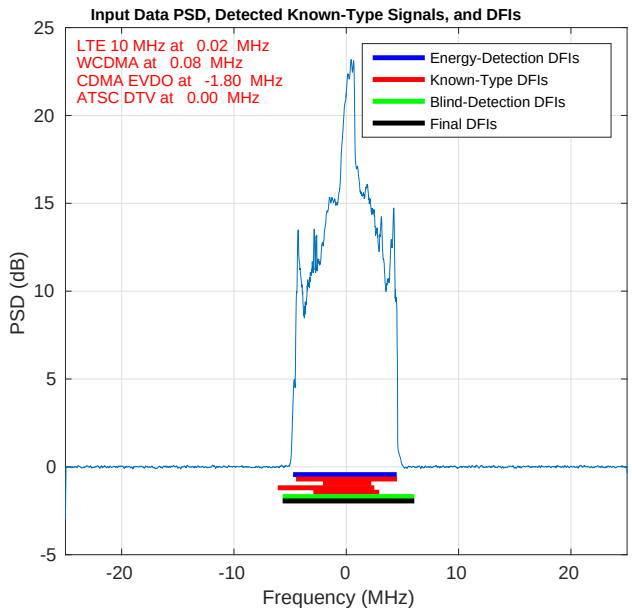

Fig. 14. Known-type detector output for an RF scene containing multiple cochannel over the air observed (OOS) signals: ATSC-DTV, CDMA EVDO, LTE, WCDMA, and CDMA. The red text indicates the decisions (CDMA is missed).

for the simulation. All signals employ independent and identically distributed data symbols. The results are summarized in Figure 16. For the low inband SNRs, the front-end ED processing stage will fail to detect the signals or will underestimate their bandwidth, leading to feature-extraction failure. However, the tunnel-based blind CSP detection step reliably detects the WB DSSS signals starting at about -10 dB due to their rather rich CS feature sets. The strided tunnel-based algorithm cannot detect the relatively NB PSK/QAM signals, however, due to the small tunnel bandwidth value of $B_t = 200$ kHz and tunnel-striding factor of four. Therefore, the NB PSK/QAM signals are not well detected until their SNR permits ED at around 3 dB.

IX. Energy Comparison

In this section, we evaluate the potential energy savings obtained by using the tunnelized CSP algorithms as opposed to the nontunnelized RAs. Expended energy is measured by counting complex multiplications, which neglects memory-access energy. However, the tunnel-based CSP algorithms are designed to avoid accessing off-chip memory by ensuring all data vectors are sufficiently short.

The computational counts are performed for four scenarios in Figure 17. The first scenario involves

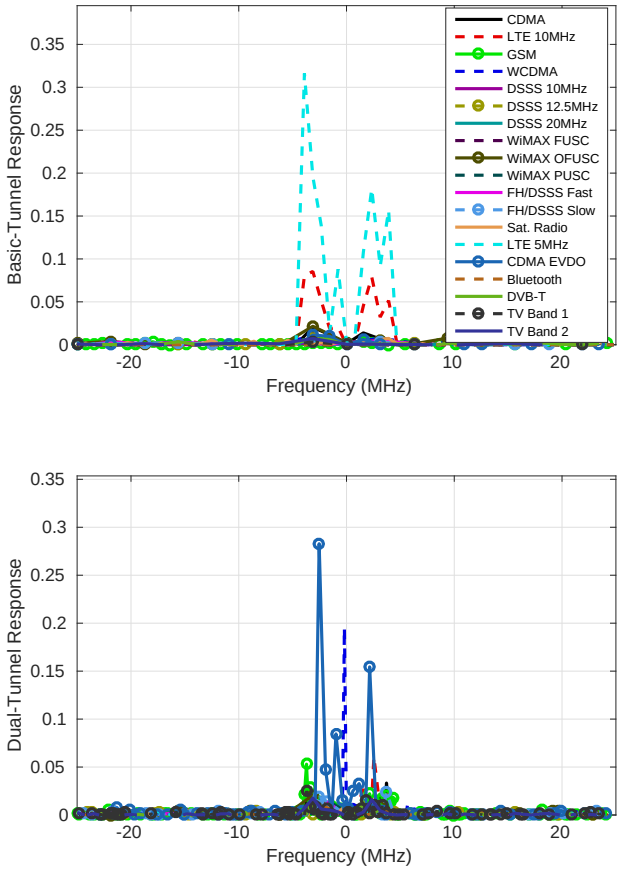

Fig. 15. Known-type tunnel responses for the RF scene shown in Figure 14. The responses are significant for each signal that is present, as well as the 5-MHz LTE signal, but are insignificant (well below threshold) for all the other known types. 5-MHz and 10-MHz LTE share CFs, and so their tunnel responses are large when either signal is present. Internal logic distinguishes between the two depending on the tunnel-response width.

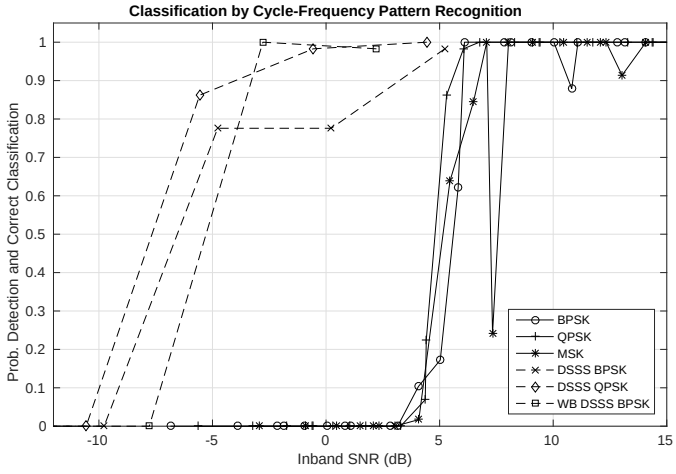

Fig. 16. Detection and classification performance for unknown-type signals using CF pattern recognition. The performance for the NB BPSK, QPSK, and MSK signals is poor for low SNR because the signals are missed by the energy-detection and strided unknown-type detection steps.

Parameter	Value
Sample Rate	50 MHz
Tunnel BW (B_t)	200 kHz ($N_t = 256$)
Block Length (T_b)	168 ms
Number of Trials	60 Per (SNR, T_b)
DFI Stride Factor	4
PSK/QAM BWs	[0.25, 2.5] MHz
PSK/QAM Pulse	SRRC
PSK/QAM SRRC Roll-Off	0.5
PSK/QAM SNRs	[-7, 23] dB
PSK/QAM per Trial	18 Distinct Signals
DSSS BW	15 MHz
DSSS SNRs	[-15, 5] dB
DSSS Pulse	SRRC
DSSS SRRC Roll-Off	0.5
DSSS T_{data}/T_{chip}	511
WB DSSS BW	30 MHz
WB DSSS SNRs	[-18, 2] dB
WB DSSS Pulse	SRRC
WB DSSS SRRC Roll-Off	0.5
WB DSSS T_{data}/T_{chip}	1023

TABLE V
MONTE-CARLO EXPERIMENT PARAMETERS FOR BLIND DETECTION OF SYNTHETIC DSSS AND PSK SIGNALS.

a 1-MHz wide signal in a 50-MHz analysis band. The counts for channelization, spectral whitening, and ED are combined into algorithm stage one, and these counts are independent of the scenario. Moreover, they are the same between the tunnel-based algorithm and the RA. However, the RA does not make use of tunnels in the subsequent algorithm stages. The KT stage has scenario-independent costs as well. We assume 22 known types, each with its own optimized tunnel-striding factor. The average cost savings is larger than a factor of ten. The UT blind detection stage also has scenario-independent costs, and here the tunnel-based algorithm is vastly less costly than the reference due to the RA's forced use of the TSM operating at the full 50-MHz input rate. Similarly, the UT classification cost for the tunnel-based algorithm is much less than for the reference due to the use of tunnels and the cyclic moment phase.

The second scenario assumes a single 10-MHz UT signal, the third three 15-MHz UT signals, and the fourth 100 50-kHz UT signals that require higher-order statistics to provide unambiguous modulation decisions (QAM/PSK signals). There is little benefit to tunneling for the last scenario, which is consistent with the design goals of the tunnel-based algorithm: low-cost detection and classification of *wideband* feature-rich signal types. The largest ben-

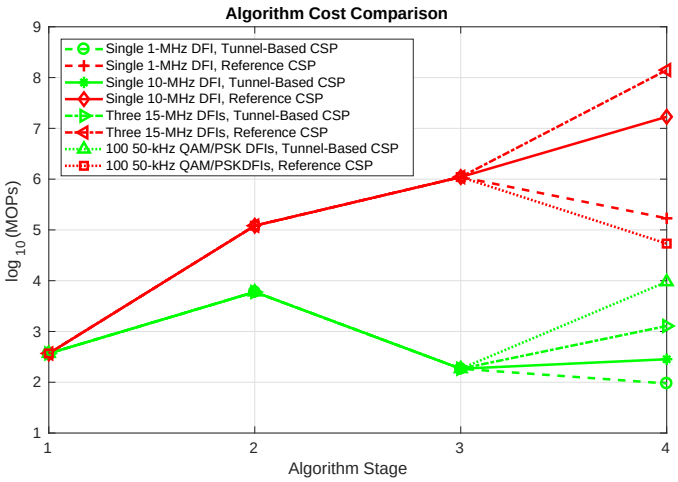

Fig. 17. Computational counts for the proposed tunnel-based CSP and reference algorithms. The initial high cost of the front-end channelization results in a large computational savings for the blind signal detection and classification stages. (See Figure 6 for stage definitions.)

efit accrues for the case of the three 15-MHz signals, where the cost difference between the two UT stages is approximately 10^5 operations.

X. Conclusions

The use of cyclostationary signal processing techniques to perform blind and nonblind signal detection, classification, and parameter estimation has been a subject of active research for the past two decades. Many capable interference-tolerant algorithmic approaches have been proposed. A serious drawback to these algorithms is their high computational cost, especially for blind processing, in which various multi-dimensional feature searches must be performed. In this paper, we have proposed a general algorithmic framework for greatly reducing the overall computational cost—and therefore the expended energy in a circuit implementation—that is especially attractive for the case of processing over-the-air observed wideband communication signals.

Appendix A
Wideband SCF Estimation Using Only Tunnels

The full NC and conjugate SCFs for arbitrary WB data can be estimated by operating only on the set of NB channelizer outputs for the data provided that the outputs are orthogonal and completely cover the data bandwidth.

Consider a provided high-rate complex-valued signal $y(t)$. The NC SCF for this signal is found by correlating the NB spectral components of $y(t)$ for all possible pairs of components,

$$\hat{S}_y^{\alpha_0}(f_0) = \langle Y_T(t, f_0 + \alpha_0/2) Y_T^*(t, f_0 - \alpha_0/2) \rangle_t \,,$$

where $Y_T(t, f)$ is the complex envelope of the spectral components in $y(t)$ centered at frequency f and with width $1/T$. Now suppose that we are given N relatively wide ($\gg 1/T$) channels of $y(t)$ to work with, and that these channels have been downconverted to complex baseband (see Figure 5). We can perform a cross-SCF analysis of the two channels $x_1(t)$ and $x_2(t)$ to determine significant cycle frequencies (CFs). We would then like to relate these cross CFs to the auto CFs for $y(t)$. The cross cyclic spectral analysis for $x_1(t)$ and $x_2(t)$ is

$$\hat{S}_{x_1 x_2}^{\alpha_*}(f_*) = \left\langle X_{1,T}(t, f_* + \alpha_*/2) X_{2,T}^*(t, f_* - \alpha_*/2) \right\rangle_t .$$

Now, the downconverted channel data is related to the original data by

$$\begin{aligned} X_{1,T}(t, f_* + \alpha_*/2) &= Y_T(t, f_* - f_1 + \alpha_*/2) \\ X_{2,T}(t, f_* - \alpha_*/2) &= Y_T(t, f_* - f_2 - \alpha_*/2) \end{aligned}$$

so that

$$\begin{aligned} \hat{S}_{x_1 x_2}^{\alpha_*}(f_*) &= \langle Y_T(t, f_* - f_1 + \alpha_*/2) \\ &\quad \times Y_T^*(t, f_* - f_2 - \alpha_*/2) \rangle_t \,. \end{aligned}$$

To find the CF for $y(t)$ that corresponds to α_* for the cross analysis of $(x_1(t), x_2(t))$, we force the desired form:

$$\begin{aligned} f_* - f_1 + \alpha_*/2 &= f_0 + \alpha_0/2 \\ f_* - f_2 - \alpha_*/2 &= f_0 - \alpha_0/2 \end{aligned}$$

which leads to $\alpha_0 = f_2 - f_1 + \alpha_*$ and $f_0 = f_* + (f_2 - f_1)/2$. Therefore, for each detected CF α_* in the cross analysis of the complex-envelope channels $(x_j(t), x_k(t))$, we add the separation between the two channels' center frequencies to obtain the corresponding CF for $y(t)$, and we add the midpoint of the channels' center frequencies to the cross-analysis frequency f_* to obtain the full-rate frequency f_0.

A benefit of using the complex-envelope channels $x_k(t)$ is that they may be decimated by an amount equal to the ratio of the channel width to the bandwidth of $y(t)$, which is equal to N_t. In this case, then, each detected CF from a cross analysis

of the decimated signals $z_k(t) = x_k(t * N_t)$ is first divided by N_t, $\alpha_0 = f_2 - f_1 + \alpha_*/N_t$.

For the conjugate SCF, we start with the basic relation

$$\hat{S}^{\beta_0}_{yy^*}(f) = \langle Y_T(t, f + \beta_0/2) Y_T(t, \beta_0/2 - f) \rangle_t \, .$$

This leads to the following expression relating the conjugate CFs of the channels to those for the original signal, $\beta_0 = f_2 + f_1 + \beta_*/N_t$.

ACKNOWLEDGMENT

The authors would like to thank the Defense Advanced Research Projects Agency for supporting this work under Contracts W911QX-12-C-0047 and FA8750-11-C-7160. They are especially grateful to Dr. William Chappell and Dr. Ted Woodward for their guidance and encouragement.

REFERENCES

[1] M. P. Anthony, J. Chuang, A. Mody, C. M. Spooner, Process for tunnelized cyclostationary to achieve low-energy spectrum sensing, PCT Patent US20160269205,

[2] (https://www.atsc.org/standards/atsc-standards/),

[3] J. Mitola, Cognitive Radio: An Integrated Agent Architecture for Software Defined Radio, Ph.D. Thesis, Royal Institute of Technology, Sweden, 2000.

[4] *Cognitive Radio Technology, Second Edition* B. Fette, Editor, Academic Press (Elsevier), ISBN: 978-0-12-374535-4, 2009.

[5] *Cognitive Radio Communications and Networks,* A. Wyglinski, M. Nekovee, and Y. Hou, Editors, Academic Press (Elsevier), ISBN: 978-0-12-374715-0, 2010.

[6] S. Haykin, "Cognitive Radio: Brain-Empowered Wireless Communications," *IEEE Journal on Sel Areas in Comm* **23**:2, Feb 2005, pp. 201–220.

[7] S. Haykin, D. Thomson, and J. Reed, "Spectrum Sensing for Cognitive Radio," *Proc of the IEEE,* **97**:5, May 2009, pp. 849–877.

[8] F. K. Jondral, "Cognitive Radio: A Communications Engineering Perspective," *IEEE Wireless Comm*, **14**:4, pp. 28-33, Aug 2007.

[9] *Standard for Cognitive Wireless Regional Area Networks,* IEEE Std. 802.22-2011, http://standards.ieee.org/about/get/802/802.22.html.

[10] T. Yucek and H. Arslan, A Survey of Spectrum Sensing Algorithms for Cognitive Radio Applications, IEEE Comm Surveys & Tutorials, **11**:1, 116-130, 2009.

[11] O. A. Dobre, A. Abdi, Y. Bar-Ness, and W. Su, "A Survey of Automatic Modulation Classification Techniques: Classical Approaches and New Trends," IET Comm, **1**:4, pp. 137-156, April 2007.

[12] G. C. Carter, "Receiver Operating Characteristics for a Linearly Thresholded Coherence Estimation Detector," *IEEE Trans Acoustics, Speech, and Signal Proc,* pp. 90–92, Feb. 1977.

[13] D. Cabric, S. M. Mishra, and R. W. Brodersen, "Implementation Issues in Spectrum Sensing for Cognitive Radio," *Conference Record of the Thirty-Eighth Asilomar Conference on Signals, Systems, and Computers,* Nov 2004, pp. 772–776.

[14] D. Cabric, "Cognitive Radios: System Design Perspective," Doctoral Dissertation, Dept. of Electrical and Computer Engr., University of California, Berkeley, Dec. 2007.

[15] C. M. Spooner, "Multiresolution White-Space Detection for Cognitive Radio," *Proc of MILCOM 2007*, Orlando, FL, Oct. 29-31, 2007.

[16] A. N. Mody et al, "Recent Advances in Cognitive Communications," *IEEE Comm Magazine*, **45**:10, pp. 54–61, Oct. 2007.

[17] P. D. Sutton, K. E. Nolan, and L. E. Doyle, "Cyclostationary Signatures in Practical Cognitive Radio Applications," *IEEE Journal on SAC*, **26**:1, pp. 13–24, Jan. 2008.

[18] C. M. Spooner *et al*, "Tunnelized Cyclostationary Processing: A Novel Approach to Low-Energy Spectrum Sensing," in *Proc of MILCOM 2013*, San Diego, CA, Nov 2013.

[19] Z. Tian, Y. Tafesse, and B. M. Sadler, "Cyclic Feature Detection With Sub-Nyquist Sampling for Wideband Spectrum Sensing," *IEEE Journal on Sel Topics in Signal Processing,* **6**:1, pp. 58–69, Feb. 2012.

[20] C. W. Lim and M. B. Wakin, "Compressive Temporal Higher Order Cyclostationary Statistics," *IEEE Trans Sig Proc*, **63**:11, pp. 2942–2956, June 2015.

[21] J. Lillington, "Slice And Dice Chunks Of Radio Spectrum," http://electronicdesign.com/analog/slice-and-dice-chunks-radio-spectrum, Dec. 2003.

[22] Y. Zhao, B. Le, and J. Reed, "Network Support: The Radio Environment Map," *Chapter 11 in Cognitive Radio Technology, Second Edition*, B. Fette, Ed., Academic Press, 2009.

[23] C. M. Spooner and N. V. Khambekar, "A Signal-Processing Perspective on Signal-Statistics Exploitation in Cognitive Radio," *Journal of Communication*, **7**:7, July 2012.

[24] W-Y Lee and I. Akyildiz, "Optimal Spectrum Sensing Framework for Cognitive Radio Networks," *IEEE Trans Wireless Comm* **7**:10, Oct. 2008, pp. 3845–3857.

[25] Z. Quan, S. Cui, A. Sayed, and H. Poor, "Optimal Multiband Joint Detection for Spectrum Sensing in Cognitive Radio Networks," *IEEE Trans Sig Proc* **57**:3, March 2009, pp. 1128–1139.

[26] P. Paysarvi-Hoseini and N. C. Beaulieu, "Optimal Wideband Spectrum Sensing Framework for Cognitive Radio Systems," *IEEE Trans Sig Proc*, **59**:3, March 2011, pp. 1170–1182.

[27] Z. Quan, W. Zhang, S. Shellhammer, and A. Sayed, "Optimal Spectral Feature Detection for Spectrum Sensing at Very Low SNR," *IEEE Trans Comm*, **59**:1, Jan. 2011, pp. 201–211.

[28] K. Hossain and B. Champagne, "Wideband Spectrum Sensing for Cognitive Radios with Correlated Subband Occupancy," *IEEE Sig Proc Letters,* **18**:1, Jan. 2011, pp. 35–38.

[29] Y. Chen, "Improved Energy Detector for Random Signals in Gaussian Noise," *IEEE Trans Wireless Comm*, **9**:2, Feb. 2010, pp. 558-563.

[30] W. Jun and B. Guangguo, "Spectrum Sensing in Cognitive Radios Based on Multiple Cumulants," *IEEE Signal Proc Letters*, **17**:8, Aug. 2010, pp. 723–726.

[31] A. Swami and B. M. Sadler, "Hierarchical Digital Modulation Classification Using Cumulants," *IEEE Trans Comm,* **48**:3, pp. 416–429, March 2000.

[32] W. A. Gardner, A. Napolitano, and L. Paura, "Cyclostationarity: Half a Century of Research," *Signal Processing*, **86**:4, pp. 639–697, 2006.

[33] B. Ramkumar, "Automatic Modulation Classification for Cognitive Radios Using Cyclic Feature Detection," *IEEE Circuits and Systems Mag*, **9**:2, pp.27–45, 2009.

[34] W. A. Gardner and C. M. Spooner. "Signal Interception: Performance Advantages of Cyclic-Feature Detectors," *IEEE Trans Comm,* **40**:1, pp. 149–159, Jan 1992.

[35] W. A. Gardner and C. M. Spooner, "Detection and Source Location of Weak Cyclostationary Signals: Simplifications of

the Maximum-Likelihood Receiver," *IEEE Trans Comm,* **41**:6, June 1993, pp. 905–916.

[36] C. M. Spooner, "Classification of Cochannel Communication Signals using Cyclic Cumulants," *Proc of the 29th Asilomar Conference on Signals, Systems, and Computers,* Oct 1995, pp. 531–536.

[37] C. M. Spooner, W. A. Brown, and G. K. Yeung, "Automatic Radio-Frequency Environment Analysis," *Proc of the 34th Asilomar Conference on Signals, Systems, and Computers,* Oct 2000, pp. 1181–1186.

[38] C. M. Spooner, "On the Utility of Sixth-Order Cyclic Cumulants for RF Signal Classification," *Proc of the 35th Asilomar Conference on Signals, Systems, and Computers,* 11/01, pp. 890–897.

[39] C. M. Spooner and R. B. Nicholls, "Spectrum Sensing Based on Spectral Correlation," *Ch. 18 in Cognitive Radio Technology, Second Edition,* Ed. B. Fette, Academic Press, 2009.

[40] W. A. Gardner, "Spectral Correlation of Modulated Signals: Part I—Analog Modulation," *IEEE Trans Comm*, **35**:6, pp. 584–594, June 1987.

[41] W. A. Gardner, W. A. Brown, and C-K Chen, "Spectral Correlation of Modulated Signals: Part II—Digital Modulation," *IEEE Trans Comm* **35**:6, pp. 595–601, June 1987.

[42] J. Lunden, V. Koivunen, A. Huttunen, and H. Poor, "Collaborative Cyclostationary Spectrum Sensing for Cognitive Radio Systems," *IEEE Trans Sig Proc*, **57**:11, Nov. 2009, pp. 4182–4195.

[43] W. A. Gardner, *Statistical Spectral Analysis*. Englewood Cliffs, NJ: Prentice-Hall, 1987.

[44] W. A. Gardner, "Exploitation of Spectral Redundancy in Cyclostationary Signals," IEEE Signal Proc Mag, **8**:2, pp. 14-36, April 1991.

[45] W. A. Gardner, "Measurement of Spectral Correlation," IEEE Trans on Acoustics, Speech, and Sig Proc, **34**:5, pp. 1111-1123, Oct. 1986.

[46] R. S. Roberts, W. A. Brown, and H. H. Loomis, Jr., "Computationally Efficient Algorithms for Cyclic Spectral Analysis," IEEE Sig Proc Mag, pp. 38-49, April 1991.

[47] W. A. Brown and H. H. Loomis, Jr., "Digital Implementations of Spectral Correlation Analyzers," IEEE Trans Sig Proc, **41**:2, pp. 703-720, Feb. 1993.

[48] A. Napolitano, *Generalizations of Cyclostationary Signal Processing,* Wiley (IEEE Press), ISBN: 978-1-119-97335-5, 2012.

[49] C. M. Spooner and W. A. Gardner, "The Cumulant Theory of Cyclostationary Time-Series, Part I: Foundation and Part II: Development and Applications," *IEEE Trans Sig Proc,* **42**:12, pp. 3387–3429, Dec. 1994.

[50] L. Izzo and A. Napolitano, "The Higher-Order Theory of Generalized Almost-Cyclostationary Time Series," *IEEE Trans Signal Proc*, **46**:11, pp. 2975–2989, Nov. 1998.

[51] P. Marchand, J-L Lacoume, and C. Le Martret, "Multiple Hypothesis Modulation Classification Based on Cyclic Cumulants of Different Orders," *Proc of ICASSP*, 1998.

[52] J. Reichert, "Automatic Classification of Communication Signals using Higher-Order Statistics," *Proc of ICASSP,* San Francisco, CA, pp. V-221–V-224, April 1992.

[53] C. Schreyogg, K. Kittel, and U. Kressel, "Robust Classification of Modulation Types using Spectral Features Applied to HMM," *Proc of MILCOM,* Monterey, CA, 1997.

[54] D. J. Thomson, "Spectrum Estimation and Harmonic Analysis," *Proc of the IEEE*, **70**:9, Sept. 1982, pp. 1055–1096.

[55] Q. Zhao and A. Swami, "A Survey of Dynamic Spectrum Access: Signal Processing and Networking Perspectives," *IEEE Trans Acoustics, Speech and Sig Proc,* **97**:5, April 2007.

[56] J. G. Proakis and M. Salehi, *Digital Communications, Fifth Edition,* Boston, MA: McGraw-Hill, 2008.

[57] E. Rebeiz *et al*, "Energy-Efficient Processor for Blind Signal Classification in Cognitive Radio Networks," *IEEE Trans Circuits and Systems*, **61**:2, pp. 587–599, Feb. 2014.

[58] https://cyclostationary.blog/data-sets/tunneling-paper-captured-data-files